Functional muscle recovery following dystrophin and myostatin exon splice modulation in aged *mdx* mice

Ngoc Lu-Nguyen[1], Arnaud Ferry[2], Frederick J. Schnell[3], Gunnar J. Hanson[3], Linda Popplewell[1], George Dickson[1,†], Alberto Malerba[1,†,*]

[1]Centres of Gene and Cell Therapy and Biomedical sciences, School of Biological Sciences, Royal Holloway-University of London, Egham, Surrey, TW20 0EX, UK.

[2]Sorbonne Université, UMRS974 INSERM, Institut de Myologie, 75013 Paris, France and Université Sorbonne Paris Cité, 75006 Paris, France.

[3]Sarepta Therapeutics, Inc., 215 First Street, Cambridge, MA 02142, USA.

Correspondence should be sent to: Alberto Malerba, Centers of Gene and Cell Therapy and Biomedical sciences School of Biological Sciences,
Royal Holloway, University of London, Egham, Surrey, TW20 0EX, UK. Tel: 44-(0)1784-443873 Email: alberto.malerba@rhul.ac.uk

Authors marked with † equally contributed to the manuscript as last authors.

Abstract

Duchenne muscular dystrophy (DMD) is a rare genetic disease affecting 1 in 3500-5000 newborn boys. It is due to mutations in the *DMD* gene with a consequent lack of dystrophin protein that leads to deterioration of myofibres and their replacement with fibro-adipogenic tissue. Out-of-frame mutations in the *DMD* gene can be modified by using antisense oligonucleotides (AONs) to promote skipping of specific exons such that the reading frame is restored and the resulting protein produced, though truncated, is functional. We have shown that AONs can also be used to knock down

myostatin, a negative regulator of muscle growth and differentiation, through disruption of the transcript reading frame, and thereby enhance muscle strength. In young *mdx* mice, combined dystrophin and myostatin exon skipping therapy greatly improved DMD pathology, compared to the single dystrophin skipping approach. Here we show that in aged (> 15-month old) *mdx* mice, when the pathology is significantly more severe and more similar to the one observed in DMD patients, the effect of the combined therapy is slightly attenuated but still beneficial in improving the disease phenotype. These results confirm the beneficial outcome of the combination approach and support its translation into DMD clinical trials.

Introduction

Duchenne muscular dystrophy (DMD) is a rare neuromuscular disease affecting 1 in 3500-5000 newborn boys worldwide (1). It is due to mutations in the *DMD* gene coding for dystrophin protein that connects the cytoplasmic actin to the dystrophin associated protein complex at the sarcolemma of the myofibres (2, 3). Loss of dystrophin in the sarcolemma weakens the stability of the myofibres such that they are prone to collapse. Muscle turn-over occurs during initial stages of the disease by activation, proliferation and differentiation of muscle stem cells (3, 4). Over time the pool of muscle stem cells is exhausted leaving muscle tissue being replaced by adipogenic and connective tissues (5). No cure is currently available for this genetic disease and therefore, individuals affected by DMD generally die in their mid-20s to early 30s mainly due to cardiac and respiratory failure (6).

Lack of dystrophin due to frameshift mutations can be modified by the use of antisense oligonucleotides (AONs). These molecules are designed to target regulatory elements of out-of-frame exons in the dystrophin pre-mRNA to restore the *DMD* reading frame and recover production of dystrophin protein, in a truncated but functional form (7). Sarepta Therapeutics, Inc. currently leads clinical trials using phosphorodiamidate morpholino oligomer (PMO) AONs. Their antisense therapeutics for exon 51 (Eteplirsen) of the *DMD* gene received an accelerated conditional approval from the Food and Drug Administration in 2016

(https://www.fda.gov/newsevents/newsroom/pressannouncements/ucm521263.htm). While an exon skipping approach has exciting potential, it is mutation specific and thereby different AONs are required to target different exons. Furthermore, the efficacy of AONs has been hampered by their modest intake by the muscle tissue (in particular the cardiac muscle). Hence, several strategies developing AONs to be conjugated to cell-penetrating peptides, aptamers or antibodies have been explored, significantly improving the uptake of AONs into the tissues (8–11).

Antisense therapeutics have been also developed to knock-down expression of myostatin, a member of the TGF-β family and a negative regulator of muscle growth and differentiation (12). Since myostatin knockout animals display a significant increase in muscle mass (12–14), many anti-myostatin strategies have been studied as therapeutic approaches for the treatment of diseases where muscle mass is reduced; for example, cancer-induced cachexia, sarcopenia, or muscle atrophy due to neuromuscular and neurological diseases (e.g. DMD, spinal muscular atrophy, amyotrophic lateral sclerosis). In preclinical approaches for DMD, systemic delivery of AAVs expressing pro-peptide for myostatin or delivery of myostatin-specific antibodies has shown encouraging results with a substantial increase in muscle mass (15–17).

We have recently reported that combining antisense therapeutics re-framing dystrophin while disrupting myostatin pre-mRNA has a synergistic effect in improving the disease (18, 19). Significant benefit was observed when AONs were systemically administered in both newborn (18) and juvenile *mdx* mice (19), the most used animal model of DMD where a point mutation in exon 23 of the murine *Dmd* gene prevents production of dystrophin protein (20). The *mdx* mouse model is a valuable tool and widely used to test *in vivo* approaches for DMD. However, the DMD phenotype is better reproduced on these animals when mice are more than 10-12 months old. From this stage onwards, cardiac and skeletal muscles (in particular the diaphragm) are remarkably dysfunctional due to severe infiltration by fibrotic and inflammatory cells (21). However, no studies have yet investigated the effect of dystrophin restoration by exon skipping in these aged *mdx* mice.

Here we compare the combination of dystrophin and myostatin exon skipping with the single dystrophin exon skipping in aged (> 15-months old) *mdx* mice. We report our findings following 10-weekly intravenous delivery of PMOs linked to a cell-penetrating B peptide (BPMOs) and provide evidence to support that simultaneous exon skipping-mediated myostatin downregulation has an additive impact on dystrophin restoration and on muscle function of treated mice.

Results

Chronic administration of antisense oligonucleotides targeting dystrophin and myostatin in aged mdx mice induces high levels of dystrophin expression

Aged (>15-month old) male *mdx* mice were intravenously injected with phosphorodiamidate morpholino oligomers (PMOs) conjugated to a cell-penetrating peptide (B-peptide). Mice received weekly injections of either 10 mg/kg BPMO-M23D targeting dystrophin (n=5) or a cocktail of 10 mg/kg BPMO-M23D and 10 mg/kg BPMO-MSTN targeting myostatin (BPMO-M23D+MSTN, n=5) for 10 consecutive weeks to potentially allow a substantial and consistent amount of dystrophin restoration. Age-matched saline-treated *mdx* (n=6) and C57BL/10J mice (n=6) were used as controls. All mice survived until the end of the experiment. Body weight of mice measured every week, showed that at this age the weight in both dystrophic and wild-type mice tended to decrease over time. *Mdx* mice lost 2.9±0.6 grams of body weight after the 10-week treatment while administration of either BPMO-M23D or the combination of the BPMOs significantly reduced the loss of body weight (losing 1.3±0.2 and 1.8±0.2 grams, $p<0.01$ and $p<0.05$ respectively, **Figure 1A**). Two weeks after the last injection, body-wide muscles were harvested and weighed. *Mdx* muscles present pseudohypertrophy due to myofibre branching and inflammation and were heavier than wild-type muscles with the ratio muscle weight/body weight significantly higher in *mdx* mice versus C57 mice for diaphragm (DIA, 4.2±0.1 vs 3.5±0.1, $p<0.05$), extensor digitorum longus (EDL, 0.47±0.04 vs 0.35±0.01, $p<0.05$), soleus (SOL, 0.46±0.02 vs 0.29±0.01, $p<0.001$) and tibialis anterior (TA, 2.4±0.1 vs 1.5±0.02, $p<0.001$), while no difference was observed in the gastrocnemius muscle (GAS, 4.96±0.14 vs 4.9±0.1, $p>0.05$). Treatment with either BPMO-M23D or the combined BPMOs did not substantially change the muscle weight of *mdx* DIA (4.2±0.11 and 4.1±0.15 respectively), EDL

(0.48±0.04 and 0.52±0.02 respectively), GAS (4.30±0.38 and 4.26±0.30 respectively), SOL (0.38±0.02 and 0.42±0.02 respectively) or TA (2.46±0.13 and 2.56±0.15 respectively), as compared to muscles of saline-treated *mdx* mice (**Figure 1B**). Two weeks after the last injection, DIA, EDL, GAS, SOL, TA, and heart muscles were collected and processed for RNA and protein extraction. Densitometric analysis of nested RT-PCR products was performed in all these skeletal and cardiac muscles. Consistent *Dmd* exon 23 skipping was observed in all skeletal muscles following BPMO-M23D delivery, ranging from 35.4±1.4% (DIA) to 60.4±3.4% (TA) of the total transcript. Administration of BPMO-M23D+MSTN led to an increase in skipping efficiency from 46.6±0.7% to 59.4±1.0% ($p < 0.0001$), as an average of all muscles analysed, with the highest enhancement observed in DIA (from 35.4±1.4% to 61.2±3.9%, $p=0.0003$) and a notable increase in the heart (from 16.4±1.6% to 27.0±1.6%, $p=0.0016$) (**Figures 2A, B**). Dystrophin protein restored as a result of the treatments was measured by immunoblot and expressed as the percentage of wild-type dystrophin quantified based on serial concentrations of C57BL/10J dystrophin protein (**Figures 2C, D**). BPMO-M23D delivery rescued 4.1±2.0% body-wide dystrophin, with an exceptional maximal level of 13.1±3.7% in SOL. In DIA and heart, dystrophin was detected at lower amounts (1.5±1.5% and 4.8±0.6%, respectively) but only when BPMO-MSTN was co-delivered. Administration of BPMO-M23D+MSTN increased body-wide level of dystrophin from 4.1±2.0% to 9.8±3.0% ($p=0.001$), and significantly improved the level in TA muscle (from 5.0±1.2% to 21.0±3.2%, $p=0.0015$) (**Figure 2D**). To complement the results obtained by western blot, we performed co-immunostaining for dystrophin and laminin in two crucial muscles, TA and DIA (**Figure 2E**). BPMO treated muscles showed dystrophin expression clearly distinguishable compared to the background of saline treated muscles and with patches of fibres expressing higher dystrophin levels. The percentage of such dystrophin positive fibres relative to total fibres (laminin positive) was quantified, confirming 35.2±2.2% and 12.9±0.6% fibres rescued in TA and DIA, respectively after BPMO-M23D administration. Co-delivery of BPMO-M23D and BPMO-MSTN increased the percentage of dystrophin positive fibres to 44.1±2.2% ($p<0.01$) in TA and 32±3% ($p<0.001$) in DIA (**Figures 2F, G**). 3.4±0.3% dystrophin positive fibres were observed in saline-treated muscles.

These data show that aged mdx mice generally lose body weight overtime and that the treatment with either BPMO-M23D or the BPMO combination reduce this bodyweight loss although no effects are observed in muscle weight. Furthermore, these data demonstrate that systemic delivery of BPMO-M23D induces a substantial skipping of dystrophin exon 23 accompanied by the production of dystrophin protein in aged mdx mice. Co-delivery of BPMO-M23D+MSTN significantly enhances exon skipping levels and increases dystrophin protein production.

Delivery of BPMOs for dystrophin and myostatin exon skipping in aged mdx mice induces detectable MSTN skipping bodywide and decrease of MSTN mRNA in diaphragm

Following densitometric analysis of nested RT-PCR products, we detected skipping of *Mstn* exon 2 in all the examined tissues at an average of 19.6±2.7%, with the lowest amount in GAS (10.4±1.1%) and the highest in DIA (35.4±11.9%) (**Figures 3A, B**). In order to assess the efficacy of the treatment in myostatin expression we performed an ELISA assay on sera of treated mice and quantitative real-time RT-PCR in TA and DIA muscles. Saline-injected *mdx* mice expressed significantly less circulating myostatin protein than wild type mice as expected, p=0.0002 (22) (**Figure 3C**). Analysis of *Mstn* mRNA via qRT-PCR consistently confirmed that the mRNA level in both DIA and TA muscles of aged *mdx* mice expressed significantly less *Mstn* compared to the wild type levels, p<0.0001 and p=0.0365 respectively. Although we did not detect any significant change between the *mdx* groups in either myostatin protein or mRNA level, only dystrophic TA muscles receiving BPMO treatment displayed a similar amount of *Mstn* RNA compared to wild type muscles (**Figures 3D, E**).

These data show that BPMO-MSTN induces detectable body-wide skipping of Mstn pre-mRNA although with different efficacy among muscles.

Dystrophin and Myostatin exon skipping ameliorates histopathological features of DMD and protects muscles of aged mdx mice

Dystrophic muscles are affected by muscle necrosis that induces myofibre turn-over, excessive fibrosis deposition and muscle weakness. Thereby, we analysed the effect of the chronic systemic

administration of BPMOs on DMD physiopathology based on these parameters. Repeated tissue degeneration-regeneration cycles were examined by measuring the number of centrally nucleated fibres (CNFs), expressed as percentage of the total fibre number. Co-staining of laminin (for myofibre sarcolemma) and DAPI (for nuclei) was used to evaluate the percentage of CNFs in the muscles. Whilst 85.3±1.4% CNFs were detected in TA of untreated *mdx* mice, administration of BPMO-M23D resulted in a statistically not significant decrease to 77.2±3.7% CNFs (p=0.07, Student t-test) in the treated muscles. Co-injection of BPMO-M23D and BPMO-MSTN reduced significantly CNFs to 74.8±2.9% (p <0.05) (**Figure 4A**) as compared to TA muscles of saline treated *mdx* mice. In DIA muscles of saline-treated *mdx* mice, only 5.9±0.4% CNFs were detected probably because this muscle is severely affected and the majority of damaged myofibres had been replaced by fibrotic tissue at the examination time. Thereby, we observed minor non-significant alterations in the percentage of CNFs following delivery of either BPMO-M23D or BPMO-M23D+MSTN in DIA muscle (**Figure 4B**). The amount of fibrosis in TA, DIA and GAS muscles of treated mice was further analysed by measuring the area covered by the staining of muscle sections for Collagen VI and by Sirius red solution for detecting Collagen I and III. In TA muscles, treatment with BPMO-M23D or with the combination of the 2 BPMOs significantly reduced the amount of Sirius red positive area from 7.2±0.8% (in saline-treated *mdx* mice) to 3.9±0.4% (p<0.05) and 4.4±0.5% (p<0.01) respectively (**Figures 4C, E**). Collagen VI staining was also reduced from 10.8±0.6% (in saline-treated *mdx* mice) to 6.5±0.7% (p<0.01) and 6.2±0.6% (p<0.001) (**Figures 4D, E**). In DIA muscle, where the area covered by connective tissue was substantially larger (52.1±2.8% of the total area in saline-treated *mdx* mice), BPMO-M23D or the combined treatment significantly reduced the collagen I and III expression to 39.5±1.9% (p<0.05) and 39.9±1.3% (p<0.001) respectively while only a statistically not significant decrease was observed for Collagen VI (p=0.07 and 0.08 with BPMO-M23D and the combined BPMOs respectively, unpaired t-test) (**Figures 4F-H**). In GAS muscles, that show an intermediate fibrotic pathological deposition, treatment with BPMO-M23D or with the combination of the 2 BPMOs significantly reduced the amount of Sirius red detected area from 25.2±2.1% (in saline-treated *mdx* mice) to 17.2±1.8% (p<0.05) and 17.8±1.3% (p<0.05) respectively (**Supplementary**

Figures 1A, C). Collagen VI expression was also reduced from 21±1% (in saline-treated *mdx* mice) to 13.3±1.1% (p<0.001) and 12.9±0.4% (p<0.001) respectively (**Supplementary Figures 1B, C**).

In order to evaluate the benefit of antisense treatment on muscle function, both a grip strength test to assess the forelimb strength and an *in situ* muscle electrophysiology to examine the function of isolated TA muscle were performed. The force generated by the forelimbs was normalised to the final bodyweight of the mice. Aged *mdx* mice had significantly weaker forelimbs compared to those of age-matched C57BL/10J mice (20.7±0.6 mN/g of body weight in C57 mice versus 10.7±0.6 mN/g in *mdx* mice, p<0.001). Treatment with either BPMO-M23D (18.1±0.6 mN/g) or with the BPMO cocktail (18±0.5 mN/g) normalised the forelimb muscle force to the level of C57 mice (p<0.001 in both cases, **Figure 5A**). *In situ* TA muscle force measurement, by electrophysiology analysis, indicated that in *mdx* mice the specific maximal force (i.e. the maximal force generated by the muscle after 150Hz stimulation normalised by the muscle weight) was almost half of the level measured in C57BL/10J mice (11.3±1.0 N/g in *mdx* mice versus 21.5±1.2 N/g in C57 mice, p<0.001). A trend towards an increase in specific maximal force was observed after treatment with either BPMO-M23D (15.2±0.8 N/g p=0.01, student t-test) or the combination of the BPMOs (14±0.7 N/g p=0.05, student t-test) (**Figure 5B**). Furthermore, untreated dystrophic muscles were susceptible to muscle damage and displayed a clear force drop following 9 eccentric contractions. The treatment with BPMO-M23D slightly improved the resistance to the eccentric contractions (from 31% to 43% of the initial maximal force, p=0.1791) whilst muscles of mice treated with the cocktail of BPMOs were substantially protected from the damage, with a resistance to eccentric contraction of about 73% of the initial maximal force (p<0.001) (**Figure 5C**).

These data show that chronic systemic injection with either BPMO-M23D or, more substantially, with BPMO-M23D+MSTN restores dystrophin expression at the level that significantly improves some aspects of the histopathology and function in TA and GAS muscles of old mdx mice. Of importance, the treatment is sufficient in DIA muscle to significantly decrease the content in collagen I and III despite its severe pathology.

Discussion

Exon skipping of *DMD* pre-mRNA has been considered a valuable approach for the treatment of DMD. A number of clinical trials based on 2'-*O*MePS or PMO chemistry of AON has been conducted, leading to the conditional approval of a PMO called Eteplirsen by the FDA for DMD treatment. However, while AON therapy targeting the restoration of dystrophin offers potential therapeutic benefit, additional adjunct therapies could further enhance the efficacy of the treatment.

We recently described the promising effects of the antisense approach combining dystrophin and myostatin exon splice modulation in dystrophic mice at 2 different stages of the disease (8, 18, 19). We showed that in both neonatal mice (from postnatal day 0) where the muscle pathology is not developed and in juvenile mice (from 6-week old) where the disease is dramatically progressed, the dual BPMO treatment restoring dystrophin and inhibiting myostatin expression has beneficial effects on respectively preventing or significanly attenuating most of the features of the disease. Here we report and confirm these positive effects in aged *mdx* mice (from 15-month old), where the pathology is significantly more severe and more similar to the one affecting DMD boys (21, 23). To our knowledge AON-cell penetrating peptide conjugates have never been tested in such a model that is both a genocopy and a more trustable representative phenocopy of DMD. Here we confirm that: (1) BPMO-M23D administration restores dystrophin protein expression in aged *mdx* mice; (2) The dual antisense treatment improves the effect of the single dystrophin exon skipping approach.

In recent years, targeting the myostatin signaling pathway has become an attractive approach to treat muscle atrophy. In DMD, it has been suggested that myostatin knockdown could enhance muscle mass and muscle strength, and reduce muscle fibrosis in *mdx* mice (17, 24). The most advanced approach to knock down myostatin is based on the use of antibodies to block the protein (i.e. Domagrozumab). However in a recent phase II clinical trial in DMD boys, this approach failed to fulfill the clinical endpoints and was terminated (https://www.pfizer.com/news/press-release/press-release-detail/pfizer_terminates_domagrozumab_pf_06252616_clinical_studies_for_the_treatment_of_duche

nne_muscular_dystrophy). The use of AONs to disrupt MSTN pre-mRNA has an advantage over protein blockage therapies as AONs are designed to target specifically the sequence of the *MSTN* gene. Therefore, antisense approaches are selective to myostatin and can minimize off-target side-effects observed in protein blockage therapies, which potentially occur due to unexpected targeting of other members of the TGF-β family (i.e. activin) (25). Skeletal muscle-derived myostatin undergoes complex post-translational modification to maintain the balance of mature/precursor protein in the bloodstream. Once this balance is disrupted, i.e. by exogenous compounds, precursor myostatin in its latent form can be activated to regain the balance, diminishing the therapeutic benefit (26). It has been also reported that circulating myostatin level is dependent on both the type of muscle dystrophies and the disease stages (22). Mariot et al showed that in atrophic muscles (i.e. of DMD patients) the myostatin level was significantly reduced compared to healthy individuals, probably to counteract the muscle wasting process (22). This was confirmed by ELISA quantification of blood serum myostatin and RT-qPCR for *Mstn* mRNA expression in our treated mice that potentially explains the lower therapeutic effect we observed in aged mice, as compared to the levels seen previously in young mice (8, 18, 19). An alternative, but not mutually exclusive, explanation is that the highly fibrotic deposition in muscles of aged *mdx* mice further hampers the AON delivery. Indeed substantial fibrotic tissue was detected in muscles of saline-treated aged mice and particularly in the gastrocnemius and the diaphragm. This was significantly reduced in tibialis anterior and gastrocnemius muscles with BPMO treatments but only marginally attenuated in the more affected diaphragm. However, we previously showed that one-year treatment with unconjugated PMO-M23D significantly reduced the fibrosis also in the diaphragm (27), suggesting that a longer-term treatment with combined BPMOs would likely be more effective in reducing fibrosis. Therefore if the lower efficacy observed in aged mice compared to younger animals is due to the fibrosis deposition, starting early a long-term treatment with BPMOs could significantly improve the dystrophin expression in the medium-long term.

Although myostatin inhibition is not efficient enough to increase the muscle mass as seen in neonatal and juvenile dystrophic mice previously (18, 19), in the dual approach it remains sufficient to improve

dystrophin production with muscles of mice treated with the combination of BPMOs consistently expressing more dystrophin than muscles of mice treated with only BPMO-M23D. Since inhibition of myostatin upregulates the Akt/mTOR/p70S6K protein synthesis pathway (28, 29), the synthesis rate of cytoplasmic proteins like dystrophin is potentially increased when a dystrophin restorative strategy such as the BPMO-M23D is co-delivered. An increased dystrophin expression could have a significant impact on stability of myofibre integrity and then on muscle regeneration and finally in fibrosis deposition as we indeed observed. Importantly, despite being less effective than in neonatal or juvenile mice, the combined antisense therapy improved dystrophin expression in diaphragm and heart muscles where the single BPMO-M23D treatment failed to induce a detectable dystrophin expression. Since most DMD patients die from cardiac and respiratory failure (6), dystrophin recovery in respiratory and cardiac muscles has obvious clinical relevance. The beneficial effects of the combined treatment were further confirmed by the fact that forelimb strength was significantly improved after treatment. As we did not measure the strength at the initial baseline and we observed a decrease in bodyweight of untreated *mdx* mice we cannot rule out that the treatments actually prevented a decrease in muscle force more than increased the strength of the mice. Notably, the observation that the function of the hindlimb muscles was protected from damaging muscle contractions only when the muscle received the combined treatment likely reflects the enhanced dystrophin expression in muscles of mice treated with the combined BPMOs. These results demonstrate that even in a challenging environment where the disease is in an advanced stage, as in the muscles of aged *mdx* mice, the combined antisense approach is beneficial and more effective than skipping dystrophin alone with BPMO-M23D. This further confirms the potential benefits of such treatment, hence suggesting possible favourable effects of a combined AON approach in clinical scenario for DMD treatment.

Materials and methods

PMOs and PMO conjugates

Both PMOs for dystrophin (5′-GGCCAAACCTCGGCTTACCTGAAAT-3′) and MSTN (5′-CAGCCCATCTTCTCCTGGTCCTGGGAAGGT-3′) skipping were prepared and conjugated to an arginine-rich cell-penetrating peptide (so-called B-peptide: RXRRBRRXRRBRXB) at the 3'-end of the PMOs by Sarepta Therapeutics, Inc. (Cambridge, Massachusetts, USA). M23D sequence binds to the donor splice site of *Dmd* exon 23 (+07 –18) (30). Sequence to skip *Mstn* exon 2 binds to an exonic splicing enhancer within the exon (+30 +1) (31). BPMOs were solubilized in ddH_2O and diluted in sterile 0.9% saline (Sigma, Dorset, UK) before injection.

Animals and experimental design

Ethical and operational permission for *in vivo* experiments was granted by the RHUL Animal Welfare Committee and the UK Home Office. This work was conducted under statutory Home Office regulatory, ethics, and licensing procedures, under the Animals (Scientific Procedures) Act 1986 (Project Licence 70/8271). 16 *mdx* (C57BL/10ScSn-Dmdmdx) and 6 C57BL/10J (Jax strain 000665) male mice were bred in house and maintained in a standard 12-hour light/dark cycle with free access to food. Fifteen to twenty-month old mice were randomized based on the age before the first injection. C57 mice were 15.0±1.0 month-old while the mean age of *mdx* group treated with saline, BPMO-M23D or the combination of BPMOs was 16.6±0.5, 16.8±2.0 and 17.6±2.0 month-old, respectively. Five *mdx* mice were injected with 200 µl of sterile saline containing either 10 mg/kg BPMO-M23D, or a combination of 10 mg/kg BPMO-M23D and 10 mg/kg BPMO-MSTN. Groups of 6 age-matched *mdx* or C57BL/10J mice were weekly injected with 200 µl of sterile saline. Mice were weighed and tail vein injected weekly for 10 consecutive weeks. Amounts of BPMOs were adjusted accordingly for the weekly injections. One week after the last injection, forelimb muscle force was evaluated by grip strength tests. *In situ* muscle force analysis and tissue collection were performed 2 weeks after the last injection.

Tissue collection

Diaphragm (DIA), extensor digitorum longus (EDL), gastrocnemius (GAS), soleus (SOL), tibialis anterior (TA), and heart were collected from treated mice soon after contractile measurements. Tissues from one side of the body were frozen immediately in liquid nitrogen for RNA and protein extraction whilst tissues from the other side were embedded in optimal cutting temperature medium (VWR, Leicestershire, UK) and frozen in liquid nitrogen-cooled isopentane (Sigma, Dorset, UK) for cryosectioning. All samples were kept at -80^{o}C until use.

RNA extraction and RT-PCR/qPCR quantifying exon skipping efficiency

RNeasy Fibrous Tissue kit (QIAgen, Manchester, UK) was used in RNA extraction as previously described (19). Briefly, tissue was homogenized using a TissueLyser II (QIAgen, Manchester, UK) and the total RNA was extracted following the manufacturer's instructions. A ND-1000 NanoDrop spectrophotometer (Thermo Scientific, Leicestershire, UK) was used for RNA quantification. GoScript Reverse Transcription System (Promega, Southampton, UK) was used to reverse transcribe 500 nanograms of RNA in a reaction supplemented with 0.5 µg oligo d(T)16 (Thermo Scientific, Leicestershire, UK) and 0.5 µg random primer (Thermo Scientific, Leicestershire, UK), and run at 25^{o}C for 5 min, 42^{o}C for 1 hour and 72^{o}C for 15 min. Four microliters of cDNA products were used as templates in semi-nested (dystrophin) or nested (myostatin) PCRs and were amplified by GoTaq Polymerase (Promega, Southampton, UK) using PCR programs: 94°C for 2 min, 30 cycles at 94^{o}C for 1 min, 57^{o}C/54^{o}C for 1 min for semi-nested *Dmd* or 56^{o}C/57^{o}C for 1 min for nested *Mstn*, 72^{o}C for 45 sec, and final extension at 72°C for 5 min. The final PCR products were loaded onto 2% agarose gels. HyperLadder IV (Bioline, London, UK) was used as a size marker. Samples were loaded in the same order in gels showing *Dmd* and *Mstn* exon skipping and for the western blot showing dystrophin expression. GeneTools Image Analysis software 4.02 (Syngene, Cambridge, UK) was used to perform densitometric analysis of gel electrophoresis. The efficiency of dystrophin or myostatin exon skipping was evaluated as the percentage of the density of skipped products against the total density of unskipped and skipped products. In qPCR for *Mstn* mRNA, cDNA was diluted at 1:20 in qPCR water (Roche, UK). Ten nanograms of diluted cDNA were then amplified using LightCycler480 SYBR

Green Master I kit (Roche, UK), according to the manufacturer's instructions. Samples were prepared in triplicates. Reactions were run on LightCycler480 System, initialised at 95°C for 5 min, followed by 45 cycles at 95°C for 15 sec, 60°C for 15 sec, 72°C for 15 sec. Relative quantification was performed against corresponding *Gapdh* housekeeping gene.

Protein extraction and western blot quantifying dystrophin expression

Immunoblot was previously described (19). Briefly, tissue was homogenized on a TissueLyser II (QIAgen, Manchester, UK) at 25 Hz for 2 x 2 min. After centrifugation (13,000 rpm, 10 min, 4°C), the supernatant was transferred to freshly pre-chilled 1.5 ml tubes and the total protein was quantified by *DC* Protein Assay (Bio-Rad, Hertfordshire, UK) using the manufacturer's instructions. Protein samples (100 µg) were loaded on 3-8% Tris Acetate NuPage gels (Life Technologies, Paisley, UK). HiMark Pre-stained Protein Ladder (Life Technologies, Paisley, UK) was used as a size marker. Gels were run at 150 V for 1.5 h and transferred in NuPage transfer buffer (Life Technologies, Paisley, UK) mixed with 10% methanol (Sigma, Dorset, UK) to HyBond nitrocellulose membranes (GE Healthcare, Little Chalfont, UK) at 30 V for 2 h. After blocking (in 5% skimmed milk, 1X PBS, 0.2% Tween-20 for 1 h), membranes were incubated overnight at 4°C with either monoclonal mouse anti-dystrophin 6C5 (1:100, Novocastra Laboratories, Newcastle upon Tyne, UK) or mouse anti-GAPDH (1:10000, Abcam, Cambridge, UK) antibody. Then membranes were incubated with secondary antibody (1:10000, LI-COR Biosciences, Cambridge, UK), goat anti-mouse IRDye800 or goat anti-rabbit IRDye680. The blots were visualised on an Odyssey Infrared Imaging System (LI-COR Biosciences, Cambridge, UK). To perform protein quantification, a mix of wild-type and *mdx* proteins to provide 0, 5, 10, 20, 40, 60, 80% of wild-type dystrophin protein was loaded in a 3-8% Tris Acetate gel. Densitometric analysis was performed using ImageJ software (NIH, Bethesda, Maryland, USA) and dystrophin positive bands were normalised to the values of corresponding GAPDH intensity and then protein expression was calculated using the standard curve made by the set of samples with increasing wild-type dystrophin protein concentrations. All reagents were from Sigma (Dorset, UK), unless stated otherwise.

Immunostaining, histology and quantification

After cryosectioning on an OTF 5000 cryostat (Bright, Huntingdon, UK), sections (10-µm thickness) were kept at -80°C until use. For the co-immunostaining for dystrophin and laminin, sections were fixed in ice-cold acetone for 10 min and blocked in 1% BSA, 1% goat serum, 0.1% Triton X-100, 1x PBS. Sections were then incubated with rat anti-laminin antibody (1:1000, Sigma, Dorset, UK) and rabbit anti-dystrophin H12 (Dys2, 1:100, (32)) antibody at 4°C, overnight. Slides were washed three times in PBS, 0.05% Tween-20 and then incubated with goat anti-rat Alexa568 and goat anti-rabbit Alexa488 (1:200, Life Biotechnologies, Paisley, UK). For Collagen VI immunostaining, rabbit anti-Collagen VI monoclonal antibody was used (1:400, Abcam, Cambridge, UK for 1h, RT) followed by 3 washings and incubation with secondary antibody goat anti-rabbit Alexa488 (1:200, Life Biotechnologies, Paisley, UK). An additional 15 min staining with 1 µg/ml 4′,6-diamidino-2-phenylindole (DAPI, Sigma, Dorset, UK) was performed prior to mounting in Mowiol 4-88 (Sigma, Dorset, UK). Co-staining of laminin and DAPI was used to quantify the % of centrally nucleated fibres. A standard protocol for PicroSirius red staining was followed to detect Collagen I and III proteins. Immunostaining for dystrophin/laminin, laminin/DAPI and for collagen VI were visualised under an epifluorescence Olympus microscope. Six non-overlapping random images at 200x magnification were captured in the largest section of each muscle. For dystrophin-positive fibre staining, counting was performed manually using ImageJ software (NIH, Bethesda, Maryland, USA). Only fibres showing a bright and continuous staining of dystrophin around the sarcolemma were considered as dystrophin-positive. The percentage of positive fibres was calculated by dividing these values by the number of laminin positive fibres within the same image field. An average of 1200 DIA and 1100 TA fibres per animal was scored. ImageJ software was also used to calculate the area of each image covered by collagen VI or by Sirius red staining. The percentage of area covered by fibrotic tissue was calculated by dividing these values by the total area of the field. All analyses were performed blinded by a single operator.

Measurement of forelimb strength

The forelimb strength was assessed using a commercial grip strength monitor (Linton Instrumentation, Norfolk, UK). Measurements were performed 5 times per mouse over a 3-day period. Mice were held by the tail, allowed to grasp a metal mesh attached to a force transducer with their forelimbs. Mice were gently pulled until they released the grip and force was recorded. Thirty-seconds were elapsed between each of 5 sequential tests per mouse per each day. Data were expressed as gram force per gram of the final body weight.

In situ tibialis anterior muscle force measurement

Mice were anesthetized by intraperitoneal injection of pentobarbital solution (60 mg/kg). Contractile properties of TA muscles were analyzed as previously described (33, 34). Briefly the knee and foot of the mouse were fixed with clamps and the distal tendon of the muscle was attached to an isometric transducer (Dual-mode muscle lever, Aurora scientific, Aurora, Canada) using a silk ligature. The sciatic nerve was isolated and distally stimulated by a bipolar silver electrode using supramaximal square wave pulses of 0.1 ms duration. All data provided by the isometric transducer were recorded and analyzed using the Dynamic Muscle Control and Analysis Software (Aurora scientific, Aurora, Canada). Isometric measurements were made at an initial length L0 (length at which maximal tension was obtained during the tetanus). Response to tetanic stimulation (pulse frequency: 150 Hz) was recorded and the maximal force was determined. For the study of the muscle resistance to eccentric contraction, a lengthening of 15% of muscle was applied for 9 consecutive stimulations at 150Hz. Maximal (isometric) force generated after each eccentric contraction is expressed as percentage of to the initial maximal force. Blind analyses were performed by the operator.

Statistical analysis

GraphPad Prism5 software (San Diego, California, USA) was used for statistical analyses. All data are shown as the means ± S.E.M; One-way ANOVA followed by Bonferroni's *post-hoc* test or by two-tailed Student's *t*-test was used to assess the statistical significance. Significant levels were considered at $*p < 0.05$, $**p < 0.01$, $***p < 0.001$.

Acknowledgements

N.L.-N., A.M., L.P., and G.D. conceived and designed the study. N.L.-N. and A.M. performed all experiments. A.F. performed *in situ* TA muscle physiology analyses. BPMO reagent for MSTN was designed by L.P. and G.D. and synthesized by F.J.S. and G.J.H. All authors contributed to result interpretation and data analysis. N.L.-N. and A.M. wrote the manuscript with input from L.P., G.D., and F.J.S. All authors read and approved the final manuscript.

The authors thank Muscular Dystrophy UK for funding the study (grant RA/893).

Conflict of interest statement

This study was funded in part by Sarepta Therapeutics, Inc. F.J.S. and G.J.H. are employees of Sarepta Therapeutics, Inc. and may own stock/options in the company.

References

1. Chung,J., Smith,A.L., Hughes,S.C., Niizawa,G., Abdel-Hamid,H.Z., Naylor,E.W., Hughes,T. and Clemens,P.R. (2015) Twenty-year follow-up of newborn screening for patients with muscular dystrophy. *Muscle Nerve*, 10.1002/mus.24880.

2. Hoffman,E.P., Brown,R.H. and Kunkel,L.M. (1987) Dystrophin: the protein product of the Duchenne muscular dystrophy locus. *Cell*, **51**, 919–28.

3. Ohlendieck,K., Ervasti,J.M., Snook,J.B. and Campbell,K.P. (1991) Dystrophin-glycoprotein complex is highly enriched in isolated skeletal muscle sarcolemma. *J. Cell Biol.*, **112**, 135–48.

4. Dickson,G., Azad,A., Morris,G.E., Simon,H., Noursadeghi,M. and Walsh,F.S. (1992) Co-localization and molecular association of dystrophin with laminin at the surface of mouse and human myotubes. *J. Cell Sci.*, **103**, 1223–33.

5. Chang,N.C., Chevalier,F.P. and Rudnicki,M.A. (2016) Satellite Cells in Muscular Dystrophy – Lost in Polarity. *Trends Mol. Med.*, **xx**, 1–18.

6. Melacini,P., Vianello,A., Villanova,C., Fanin,M., Miorin,M., Angelini,C. and Dalla Volta,S. (1996) Cardiac and respiratory involvement in advanced stage Duchenne muscular dystrophy. *Neuromuscul. Disord.*, **6**, 367–376.

7. Baker,B.F. and Monia,B.P. (1999) Novel mechanisms for antisense-mediated regulation of gene expression. *Biochim Biophys Acta*, **1489**, 3–18.

8. Malerba,A., Kang,J.K., McClorey,G., Saleh,A.F., Popplewell,L., Gait,M.J., Wood,M.J. and Dickson,G. (2012) Dual Myostatin and Dystrophin Exon Skipping by Morpholino Nucleic Acid Oligomers Conjugated to a Cell-penetrating Peptide Is a Promising Therapeutic Strategy for the Treatment of Duchenne Muscular Dystrophy. *Mol. Ther. Nucleic Acids*, **1**, e62.

9. Yin,H., Moulton,H.M., Seow,Y., Boyd,C., Boutilier,J., Iverson,P. and Wood,M.J. a (2008) Cell-penetrating peptide-conjugated antisense oligonucleotides restore systemic muscle and cardiac dystrophin expression and function. *Hum. Mol. Genet.*, **17**, 3909–18.

10. Lehto,T., Alvarez,A.C., Gauck,S., Gait,M.J., Coursindel,T., Wood,M.J. a, Lebleu,B. and Boisguerin,P. (2014) Cellular trafficking determines the exon skipping activity of Pip6a-PMO in mdx skeletal and cardiac muscle cells. *Nucleic Acids Res.*, **42**, 3207–3217.

11. Ezzat,K., Aoki,Y., Koo,T., McClorey,G., Benner,L., Coenen-Stass,A., O'Donovan,L., Lehto,T., Garcia-Guerra,A., Nordin,J., *et al.* (2015) Self-Assembly into Nanoparticles Is Essential for Receptor Mediated Uptake of Therapeutic Antisense Oligonucleotides. *Nano Lett.*, **15**, 4364–4373.

12. McPherron,A.C., Lawler,A.M. and Lee,S.J. (1997) Regulation of skeletal muscle mass in mice by a new TGF-beta superfamily member. *Nature*, **387**, 83–90.

13. Mosher,D.S., Quignon,P., Bustamante,C.D., Sutter,N.B., Mellersh,C.S., Parker,H.G. and Ostrander,E. a (2007) A mutation in the myostatin gene increases muscle mass and enhances racing performance in heterozygote dogs. *PLoS Genet.*, **3**, e79.

14. McPherron, a C. and Lee,S.J. (1997) Double muscling in cattle due to mutations in the myostatin gene. *Proc. Natl. Acad. Sci. U. S. A.*, **94**, 12457–61.

15. Bogdanovich,S., Krag,T.O.B., Barton,E.R., Morris,L.D., Whittemore,L. and Ahima,R.S. (2002) Functional improvement of dystrophic muscle by myostatin blockade. *Nature*, **420**, 418–421.

16. Latres,E., Pangilinan,J., Miloscio,L., Bauerlein,R., Na,E., Potocky,T.B., Huang,Y., Eckersdorff,M., Rafique,A., Mastaitis,J., *et al.* (2015) Myostatin blockade with a fully human monoclonal antibody induces muscle hypertrophy and reverses muscle atrophy in young and aged mice. *Skelet. Muscle*, **5**, 34.

17. Qiao,C., Li,J., Jiang,J., Zhu,X., Wang,B., Li,J. and Xiao,X. (2008) Myostatin propeptide gene delivery by adeno-associated virus serotype 8 vectors enhances muscle growth and ameliorates dystrophic phenotypes in mdx mice. *Hum. Gene Ther.*, **19**, 241–254.

18. Lu-Nguyen,N.B., Jarmin,S. a, Saleh,A.F., Popplewell,L., Gait,M.J. and Dickson,G. (2015) Combination Antisense Treatment for Destructive Exon Skipping of Myostatin and Open Reading Frame Rescue of Dystrophin in Neonatal mdx Mice. *Mol. Ther.*, **23**, 1341–1348.

19. Lu-Nguyen,N., Malerba,A., Popplewell,L., Schnell,F., Hanson,G. and Dickson,G. (2017) Systemic Antisense Therapeutics for Dystrophin and Myostatin Exon Splice Modulation Improve Muscle Pathology of Adult mdx Mice. *Mol. Ther. - Nucleic Acids*, **6**, 15–28.

20. Bulfield,G., Siller,W.G., Wight,P. a and Moore,K.J. (1984) X chromosome-linked muscular dystrophy (mdx) in the mouse. *Proc. Natl. Acad. Sci. U. S. A.*, **81**, 1189–1192.

21. Pastoret,C. and Sebille,A. (1995) Mdx Mice Show Progressive Weakness and Muscle Deterioration With Age. *J. Neurol. Sci.*, **129**, 97–105.

22. Mariot,V., Joubert,R., Hourdé,C., Féasson,L., Hanna,M., Muntoni,F., Maisonobe,T., Servais,L., Bogni,C., Le Panse,R., *et al.* (2017) Downregulation of myostatin pathway in neuromuscular diseases may explain challenges of anti-myostatin therapeutic approaches. *Nat. Commun.*, **8**.

23. Stedman,H., Sweeney,H. and Shrager,J. (1991) The mdx mouse diaphragm reproduces the degenerative changes of Duchenne muscular dystrophy. *Nature*.

24. Bogdanovich,S., Krag,T.O.B., Barton,E.R., Morris,L.D., Whittemore,L.-A., Ahima,R.S. and Khurana,T.S. (2002) Functional improvement of dystrophic muscle by myostatin blockage. *Nature*, **420**, 418–421.

25. Han,H.Q., Zhou,X., Mitch,W.E. and Goldberg,A.L. (2013) Myostatin/activin pathway antagonism: Molecular basis and therapeutic potential. *Int. J. Biochem. Cell Biol.*, **45**, 2333–2347.

26. Lee,S.-J. (2004) Regulation of muscle mass by myostatin. *Annu. Rev. Cell Dev. Biol.*, **20**, 61–86.

27. Malerba,A., Boldrin,L. and Dickson,G. (2011) Long-term systemic administration of unconjugated morpholino oligomers for therapeutic expression of dystrophin by exon skipping in skeletal muscle: implications for cardiac muscle integrity. *Nucleic Acid Ther.*, **21**, 293–8.

28. Lipina,C., Kendall,H., McPherron,A.C., Taylor,P.M. and Hundal,H.S. (2010) Mechanisms involved in the enhancement of mammalian target of rapamycin signalling and hypertrophy in skeletal muscle of myostatin-deficient mice. *FEBS Lett.*, **584**, 2403–2408.

29. Wang,Q. and McPherron,A.C. (2012) Myostatin inhibition induces muscle fibre hypertrophy prior to satellite cell activation. *J. Physiol.*, **590**, 2151–65.

30. Gebski,B.L., Mann,C.J., Fletcher,S. and Wilton,S.D. (2003) Morpholino antisense oligonucleotide induced dystrophin exon 23 skipping in mdx mouse muscle. *Hum. Mol. Genet.*, **12**, 1801–1811.

31. Kang,J.K., Malerba,A., Popplewell,L., Foster,K. and Dickson,G. (2011) Antisense-induced myostatin exon skipping leads to muscle hypertrophy in mice following octa guanidine morpholino oligomer treatment. *Mol. Ther.*, **19**, 159–164.

32. Sherratt,T.G., Vulliamy,T. and Strong,P.N. (1992) Evolutionary conservation of the dystrophin central rod domain. *Biochem J*, **287**, 755–759.

33. Hourdé,C., Joanne,P., Medja,F., Mougenot,N., Jacquet,A., Mouisel,E., Pannerec,A., Hatem,S., Butler-browne,G., Agbulut,O., *et al.* (2013) Voluntary Physical Activity Protects from Susceptibility to Skeletal Muscle Contraction e Induced Injury But Worsens Heart Function in mdx Mice. *Am. J. Pathol.*, **182**, 1509–1518.

34. Stantzou,A., Ueberschlag-Pitiot,V., Thomasson,R., Furling,D., Bonnieu,A., Amthor,H. and Ferry,A. (2017) Effect of constitutive inactivation of the myostatin gene on the gain in muscle strength during postnatal growth in two murine models. *Muscle Nerve*, **55**, 254–261.

Legends to figures

Figure 1: Dystrophin restored by BPMO-M23D or the combined BPMO delivery reduces body loss in aged mdx mice but has no effect on muscle weight. (a) Body weight, assessed weekly and normalised to the initial weight, indicates that both the BPMO-M23D and the combined BPMO treatments reduced the loss of body weight compared to mice treated with saline. (b) Muscle mass of diaphragm (DIA), extensor digitorum longus (EDL), gastrocnemius (GAS), soleus (SOL) and tibialis anterior (TA) measured after sample collection was unchanged after BPMO treatments. Data are expressed as means ± S.E.M; n = 5-6 per group. Statistical analysis was two-tailed Student's *t*-test and comparisons were with *mdx* untreated group. Significant levels were set at *p < 0.05, **p < 0.01, ***p < 0.001.

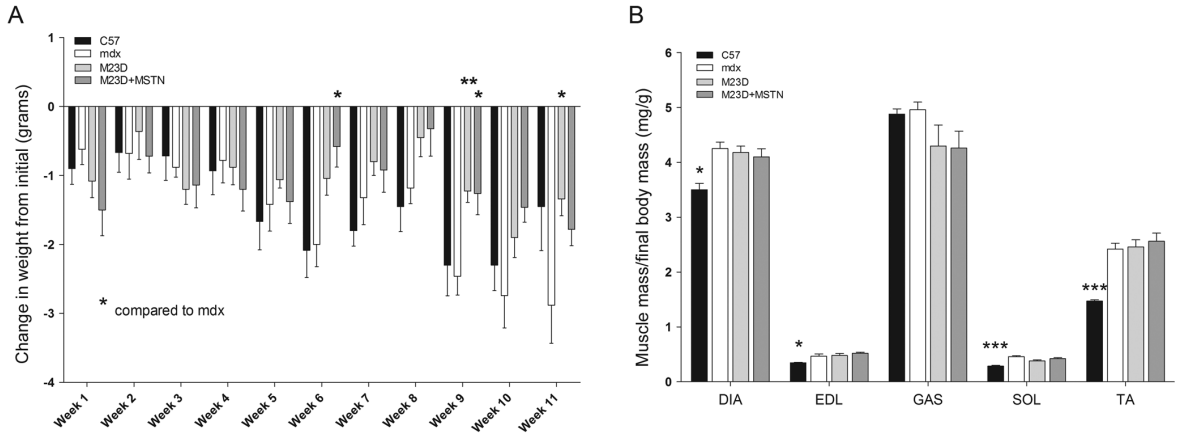

Figure 2: BPMO-M23D treatment induces efficient exon skipping of dystrophin and body-wide dystrophin restoration that is enhanced by co-delivery of BPMO-MSTN. (a) Semi-nested dystrophin RT-PCR products from diaphragm (DIA), extensor digitorum longus (EDL), gastrocnemius (GAS), soleus (SOL) and tibialis anterior (TA) and Heart were loaded on 2% agarose gels. Each lane displays the result from an individual muscle. C57, *mdx* and no template RT-PCR controls for DIA and TA are also shown. HyperLadder IV was used as a molecular size marker. Exons included in each band of PCR products are shown to the left of the gels. (b) Levels of exon skipping in each muscle type and averaged skipping of all muscles observed after the different BPMO treatments are displayed. The skipping efficiency for dystrophin, evaluated using densitometric analysis of RT-PCR products, is expressed as percentage of the density of skipped products compared to the density of the sum of skipped and unskipped products. (c) Western blot analysis in DIA, EDL, GAS, SOL, TA, and Heart muscles shows dystrophin expression after BPMO-M23D and combined BPMO-M23D+MSTN treatment in *mdx* mice. Each lane is a sample from an individual mouse. Proteins from type-matched muscle of saline-injected C57 and *mdx* mice were loaded as controls. GAPDH was used as loading control for western blot. (d) The intensity of dystrophin bands was quantified and normalised to the intensity of the corresponding GAPDH band. Results, expressed as percentage of C57 values obtained using a wild-type standard curve, show that the co-delivery of BPMOs enhanced the dystrophin expressed by the single BPMO-M23D treatment. Results of individual muscle types and the average of all muscles are shown. (e) Representative images of immunostaining for dystrophin (green) and laminin (red) expression in TA and DIA muscles are shown. Nuclei were counterstained with DAPI (blue). Scale bar: 200 μm. (f, g) The percentage of dystrophin positive fibres detected after immunostaining was quantified and expressed as percentage of laminin positive fibres. Statistical comparison was two-tailed Student's *t* test in b and d and one-way Anova test with Bonferroni *post-hoc* test in f and g; $^{**}p < 0.01$, $^{***}p < 0.001$. Data are expressed as means ± S.E.M; n = 5 per group.

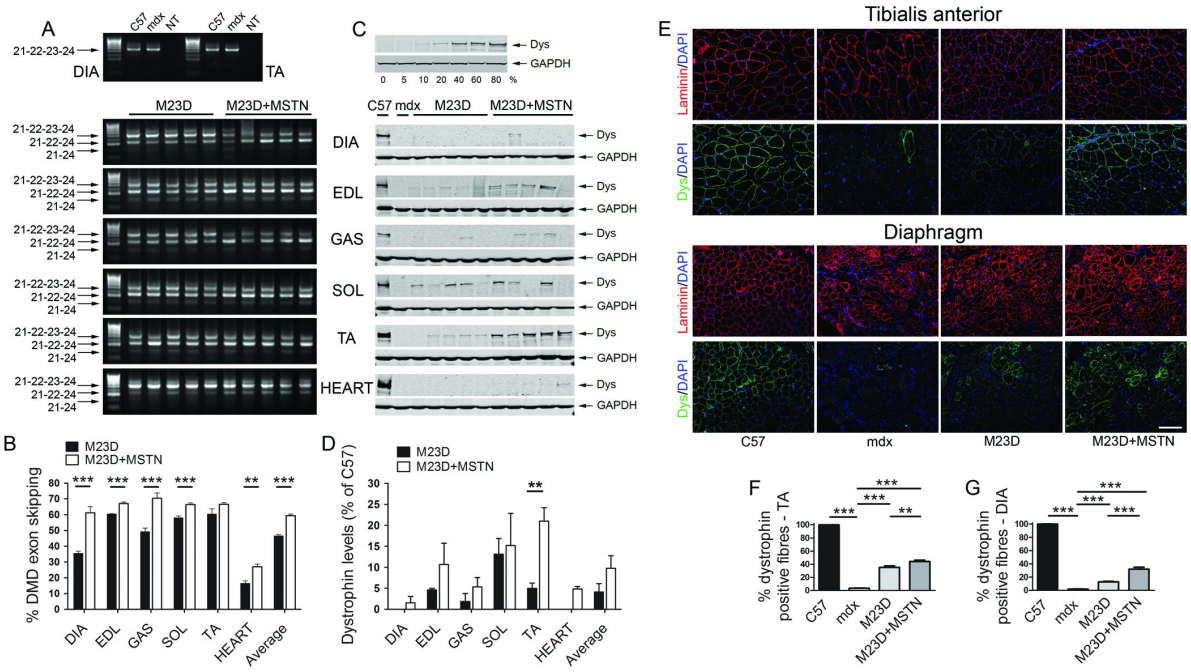

Figure 3: Chronic systemic delivery of BPMOs induces detectable exon skipping of myostatin. (a) Nested myostatin RT-PCR products from diaphragm (DIA), extensor digitorum longus (EDL), gastrocnemius (GAS), soleus (SOL), tibialis anterior (TA) and heart were loaded on 2% agarose gels. Each lane shows the result from an individual muscle. HyperLadder IV was used as a molecular size marker. Exons included in each band of PCR products are shown to the right of the gels. (b) Levels of exon skipping in each muscle types and averaged skipping of all muscles observed after the BPMO treatment are displayed. The skipping efficiency for myostatin, evaluated using densitometric analysis of RT-PCR products, is expressed as percentage of the density of skipped products compared to the density of the sum of skipped and unskipped products. (c) ELISA of circulating myostatin protein in blood serum collected from treated and untreated mice. (d) Real time RT-PCR detecting *Mstn* mRNA in DIA muscles, normalised to the *Gapdh* expression. (e) Real time RT-PCR detecting *Mstn* mRNA in TA muscles, normalised to the *Gapdh* expression. Data are expressed as means ± S.E.M; n = 5 per group. In (b-e) statistical analysis was one-way Anova test with Bonferroni *post-hoc* test, *$p < 0.05$, **$p < 0.01$, ***$p < 0.001$.

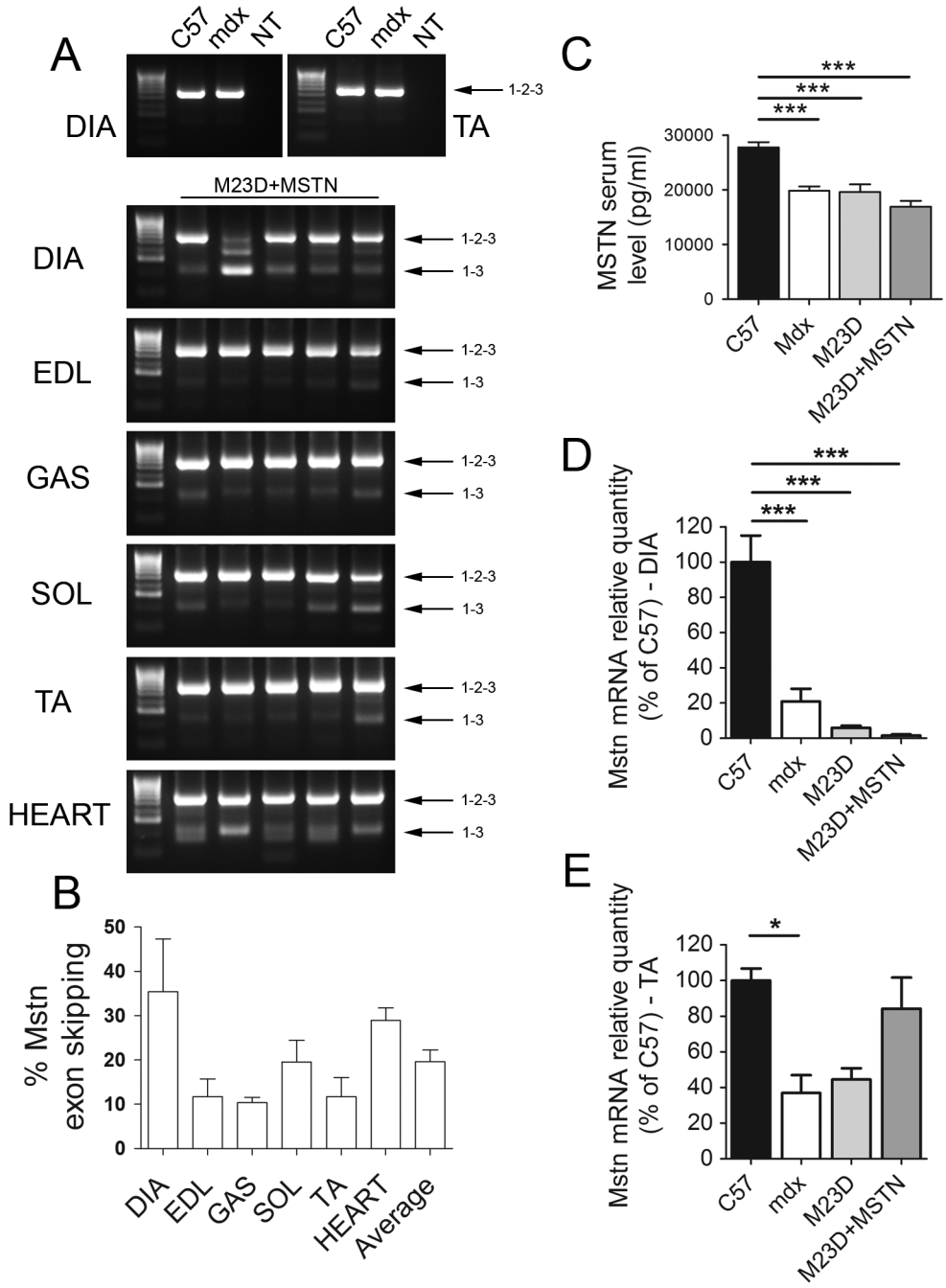

Figure 4: BPMO administration improves histopathological and functional features of dystrophic muscles. (a, b) Immunofluorescence staining for laminin and DAPI was used to quantify the percentage of fibres with one or more central nuclei (CNF: centrally nucleated fibres). Five random fields per muscle were analysed. Results are expressed as percentage of the total fibres. (c-h) Sirius red staining and immunostaining for collagen VI were performed to evaluate muscle fibrosis in sections of treated tibialis anterior (TA) and diaphragm (DIA) muscles. Scale bar: 200 µm. The area covered by the staining was quantified and analysed with NIH ImageJ. Both BPMO-M23D and the co-delivery of BPMOs reduced collagen deposition in TA (c-d) and DIA (f-g) muscles. (e, h) Representative images were captured in the largest sections of treated muscles. Data are shown as means ± S.E.M; n = 5-6 per group. Statistical comparison was one-way Anova test with Bonferroni *post-hoc* test in (a-d) and (f, g); *p < 0.05, **p < 0.01, ***p < 0.001, ns: not significant.

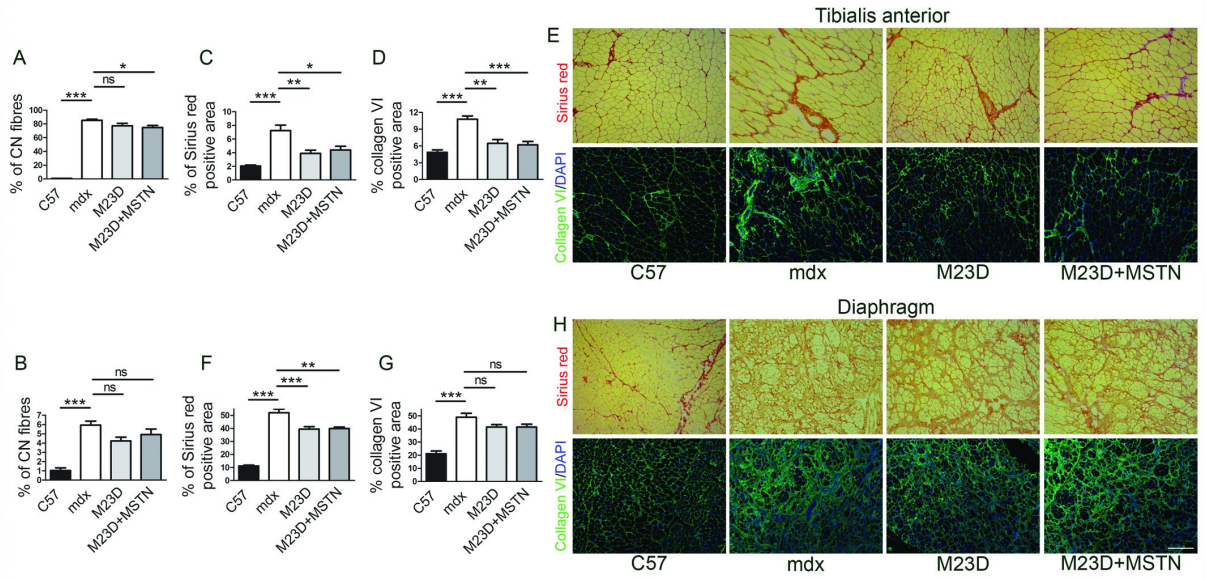

Figure 5: BPMO administration improves contractile properties of dystrophic muscles

(a) Forelimb muscle force was evaluated by grip strength test, normalised to the final body weight and expressed as gram force per gram of body weight. Results show that dystrophin produced by either BPMO-M23D or the co-delivery of BPMOs improves muscle strength in treated mice. (b) *In situ* tibialis anterior (TA) muscle physiology was performed in treated mice under terminal anesthesia. Treatment with BPMOs induces small changes in the specific maximal force detected in TA muscles. (c) Resistance to the damage provided by 9 consecutive eccentric contractions was significantly increased after treatment with the combination of BPMO-M23D and BPMO-MSTN. * and # are used to show statistical difference between *mdx* and C57 mice or *mdx* and combined BPMOs treatment respectively. Data are presented as means ± S.E.M; n = 5-6 per group. Statistical comparison was one-way ANOVA test with Bonferroni's *post-hoc* test; ***p < 0.001, ###p < 0.001, #p < 0.05, ns: not significant.

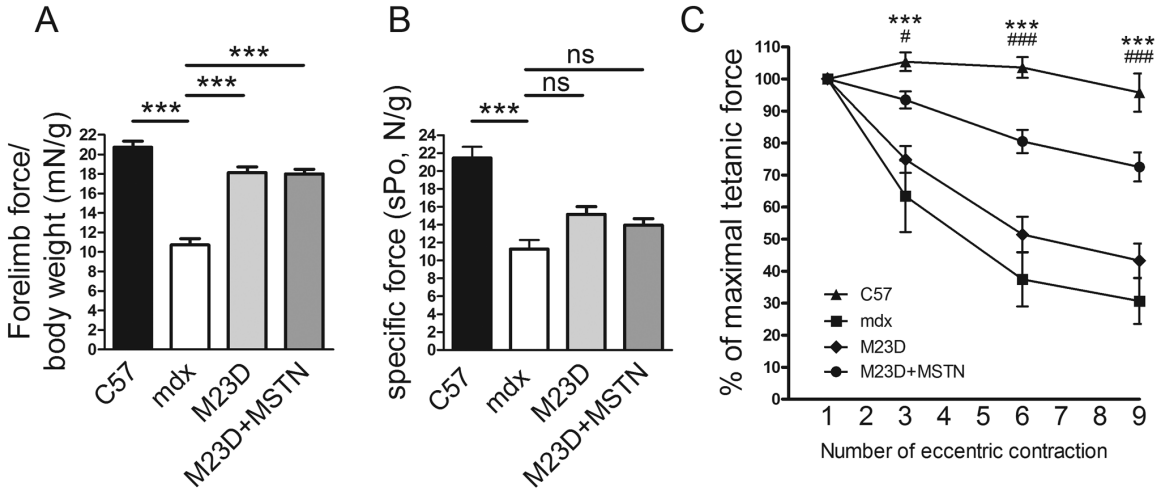

Abbreviations

DMD: Duchenne muscular dystrophy

MSTN: myostatin

PMO: phosphorodiamidate morpholino oligomer

AON: Antisense oligonucleotides

CNF: Centrally nucleated fibres

TA: tibialis anterior

DIA: diaphragm

EDL: extensor digitorum longus

SOL: Soleus

GAS: Gastrocnemius